ACS OMEGA

Open Access

http://pubs.acs.org/journal/acsodf

Article

Electroreduction of La^{3+} Ions on a Nickel-Based Cathode in a Fluoride System

Kailei Sun, Linsheng Luo, and Xu Wang*

Cite This: *ACS Omega* 2025, 10, 25007−25013

Read Online

ACCESS | Metrics & More | Article Recommendations

ABSTRACT: The regeneration and utilization of La from lanthanum thermal reduction of rare earth slag are essential for the high-value recovery of secondary rare earth resources. Reduction of lanthanum in fluoride molten salt systems by using active electrodes is a promising technique. In this study, electroreduction of La^{3+} ions on the surface of an active Ni cathode in a fluoride system was analyzed using cyclic voltammetry, square-wave voltammetry, and chronoamperometry. Scanning electrochemical microscopy (SECM) was used to analyze the current response and change in La^{3+} ions on the surface of the Ni electrode substrate. The products formed on the Ni cathode surface, upon electrolysis at a constant potential difference of 4.1 V, were analyzed and characterized using an electron probe technique. The results showed that electrochemical reduction of La^{3+} ions at the Ni cathode in the $(LiF\text{-}LaF_3)_{eut.}\text{-}La_2O_3$ molten system at 1223 K proceeded through two steps, i.e., $La^{3+} + e \rightarrow La^{2+}$ and $La^{2+} + 2e \rightarrow La$. The reduction of La^{3+} ions at the cathode was transiently nucleated and diffusion controlled with a diffusion coefficient of approximately 1.33×10^{-5} $cm^2 \cdot s^{-1}$. With a negative shift in the Ni electrode potential, the banded two-dimensional nucleation region on the cathode surface continued to expand. Further, the three-dimensional (3D) nucleation active points also increased and became uniformly distributed. The La^{3+} ions in the system were fully activated when the Ni electrode potential was in the range of −0.95 to 0.95 V (vs Ag/AgCl). This protocol yielded an alloy product mainly constituting the $LaNi_3$ and $LaNi_5$ phases.

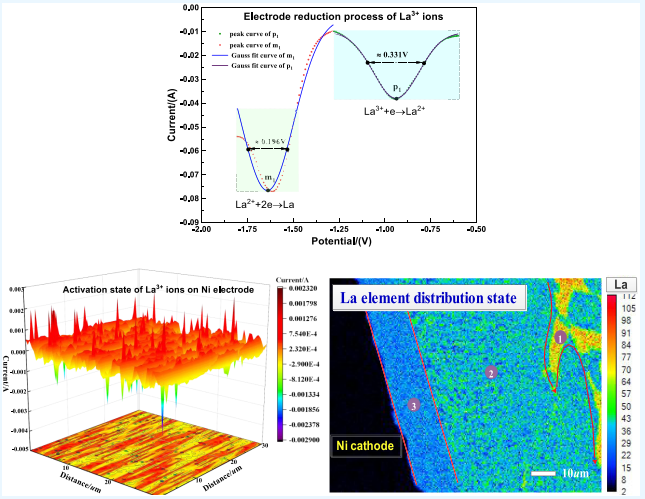

1. INTRODUCTION

Rare earth slag is generated during thermal reduction of rare earth metals and alloys, and an efficient extraction of the valuable metals contained therein has been of great concern.[1] Lanthanum−samarium slag, obtained during the process of samarium metal production by the lanthanum thermal reduction method, is mainly composed of La_2O_3 and a small amount of Sm_2O_3. At present, the industrial treatment of lanthanum−samarium slag involves acid/alkali dissolution followed by extraction to recover the rare earth elements La and Sm. However, this process generates a large amount of acid, alkali, and water as waste products, creating considerable pressure on the environment.[2] Therefore, it is necessary to explore other methods for efficient separation and regeneration of La from lanthanum−samarium slag for recycling rare earth resources.[3]

This study proposes a strategy for the treatment of lanthanum−samarium slag by the molten salt electrochemical method, using active nickel as a self-consuming cathode and electrolysis of lanthanum oxide present in the slag to produce LaNi intermediate alloys, which offers the advantages of a short process flow, high efficiency, no waste products, and environmental friendliness.[4] Currently, the main high-temperature carriers available for the electrochemical reduction of La^{3+} ions include fluoride[5−7] and chloride molten salt systems.[8−10] Regarding their efficiency, the fluoride medium has higher stability and current efficiency than the chloride medium, and the graphite anode products (mainly CO and CO_2) of the former are easier to handle and environmentally friendly.[11,12] The primary objective of this work is to explore the mechanism of the electroreduction of La^{3+} ions at a reactive nickel-based cathode in the $(LiF\text{-}LaF_3)_{eut.}\text{-}La_2O_3$ system. The activation pattern of La^{3+} ions on the surface of the Ni electrode was studied by scanning electrochemical microscopy (SECM). Constant potential electrolysis was used to prepare La−Ni

Received: March 21, 2025
Revised: May 24, 2025
Accepted: May 27, 2025
Published: June 5, 2025

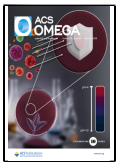

alloys, and the electrolysis products were characterized to analyze the alloying of La^{3+} ions on the Ni electrode surface and to provide a theoretical basis for further optimization of the electroreduction system.

2. EXPERIMENTAL PRINCIPLES AND METHODS

Analytically pure LiF, LaF_3, and La_2O_3 were dried at 473 K under a high-purity argon atmosphere. LiF/LaF_3 = 75/25 (eutectic mass ratio) was mixed with a 2% mass fraction of La_2O_3 and heated to 1223 K for complete melting. A platinum wire (Φ1 mm, 99.99%), a nickel wire (Φ1 mm, 99.99%), and a tungsten rod (Φ8 mm, 99.99%) were used as reference, working, and auxiliary electrodes, respectively. Cyclic voltammetry, square-wave voltammetry, and chronoamperometric analysis of the $(LiF\text{-}LaF_3)_{eut.}\text{-}La_2O_3$(2% mass fraction) system were performed by using an electrochemical workstation (AUTOLAB PGSTAT302). A four-electrode system (Ni-based working electrode, platinum wire counter electrode, Ag/AgCl reference electrode, and ultramicroprobe electrode) was constructed, and a scanning electrochemical analysis workstation (VersaSCAN SVET, Princeton) was used to analyze the current response pattern of La^{3+} ions on the surface of the Ni cathode in the generate-collect mode at a temperature of 298 K (Figure 1). A

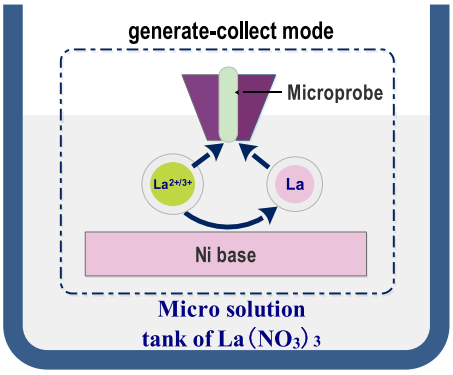

Figure 1. Schematic of the scanning electrochemical microscopy analysis mode.

graphite crucible was used as the electrolytic cell, and the alloy products were obtained by electrolysis at a constant potential of 4.1 V for 2 h in the $(LiF\text{-}LaF_3)_{eut.}\text{-}La_2O_3$ molten salt system at 1223 K. Nickel rods were used as the cathode (Φ10 mm, 99.99%), and graphite rods as the anode (Φ10 mm, spectroscopically pure). The products were characterized and analyzed by scanning electron microscope (SEM) and electron probe microanalysis (EPMA).

3. RESULTS AND DISCUSSION

3.1. Analysis of the Electrical Reduction Process of La^{3+} Ions on the Ni Cathode. *3.1.1. Analysis of Cyclic and Square-Wave Voltammetry.* Cyclic voltammetric analysis of the $(LiF\text{-}LaF_3)_{eut.}\text{-}La_2O_3$ system was performed, and the results are shown in Figure 2. The blue and red dotted lines in the figure show the cyclic voltammetry curves of $(LiF\text{-}LaF_3)_{eut.}$ obtained by scanning rates of 100 and 200 mV/s at 1223 K temperature. The consistency of the CV curves and the positions of the oxidation/reduction peaks at different scanning rates confirm the stability and consistency of the electrode reaction. All of them showed one set of corresponding reduction/oxidation peaks (n/n'), and the onset potential of the reduction peak n

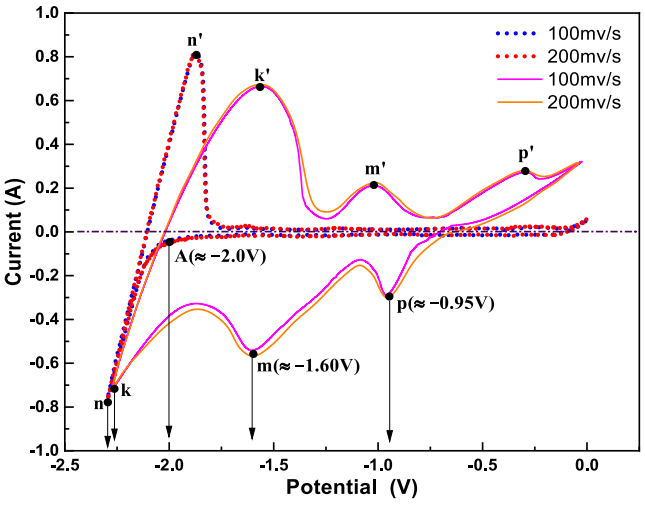

Figure 2. Cyclic voltammetry curve of the $(LiF\text{-}LaF_3)_{eut.}\text{-}La_2O_3$ (2 wt %) system (Temperature 1223 K; Pt reference electrode, Φ1 mm; Ni working electrode, Φ2 mm; W auxiliary electrode, Φ10 mm).

(attributed to $Li^+ + e \rightarrow Li$) was approximately −2.0 V (vs Pt), which indicated that the $(LiF\text{-}LaF_3)_{eut.}$ system was in an active state (i.e., Li^+ ions participate in cathodic reactions to reduce to Li) when the potential was more negative than −2.0 V, whereas the system remained stable in the range of 0 to −2.0 V. The purple and brown solid lines represent the cyclic voltammetry curves of $(LiF\text{-}LaF_3)_{eut.}$ system with the addition of 2% mass fraction of La_2O_3 at scanning rates of 100 mV/s and 200 mV/sl; three sets of corresponding reduction/oxidation peaks (k/k', m/m', p/p') appeared in the scanning range of 0 to −2.25 V. The reduction peak k corresponds to the activation of $(LiF\text{-}LaF_3)_{eut.}$ system, which means Li^+ ions in the mixed medium of LiF and LaF_3 are reduced at the cathode. The peaks m and p were attributed to the reduction of La^{3+} ions after the incorporation of La_2O_3 into $(LiF\text{-}LaF_3)_{eut.}$.The peripheral valence electrons of La are $5d^16s^2$, where the energy level of the 5*d* layer is higher than that of the 6s layer, which indicates that the reduction peaks m[approximately −1.60 V(vs Pt)] and p[approx. −0.95 V(vs Pt)] correspond to the reduction processes $La^{3+} + e \rightarrow La^{2+}$ and $La^{2+} + 2e \rightarrow La$, respectively.

To further confirm the reduction of La^{3+} ions, a square-wave voltammetric analysis of the $(LiF\text{-}LaF_3)_{eut.}\text{-}La_2O_3$ system was performed, and the results are shown in Figure 3. The reduction of m_1(≈−1.60 V), p_1(≈−0.95 V), and peaks A_1(≈−2.0 V) shown in Figure 3(a) corresponds to the of peaks m, p, and onset potential A of peak n, obtained from cyclic voltammetric analysis (Figure 2). Square-wave voltammetry uses AC-superimposed square-wave pulse potential scanning to measure the current response. The synergistic effect of pulse timing design (background suppression), electrochemical enrichment (signal amplification), and electronic optimization (noise filtering) effectively distinguishes the Faraday current from the charging current, enhancing the strength of the transient Faraday current response. Therefore, starting point A of the reduction peak n in Figure 2 can be observed in Figure 3, and the reduction current of the square-wave voltammetry curve gradually increases with a further negative shift of the scanning potential. This corresponds to the A → n stage in the cyclic voltammetry curve of Figure 2. In cyclic voltammetry sets, a closed current−potential curve is formed by reversing the scanning potential, allowing for the observation of oxidation/reduction peaks n/n'. In contrast,

https://doi.org/10.1021/acsomega.5c02626
ACS Omega 2025, 10, 25007−25013

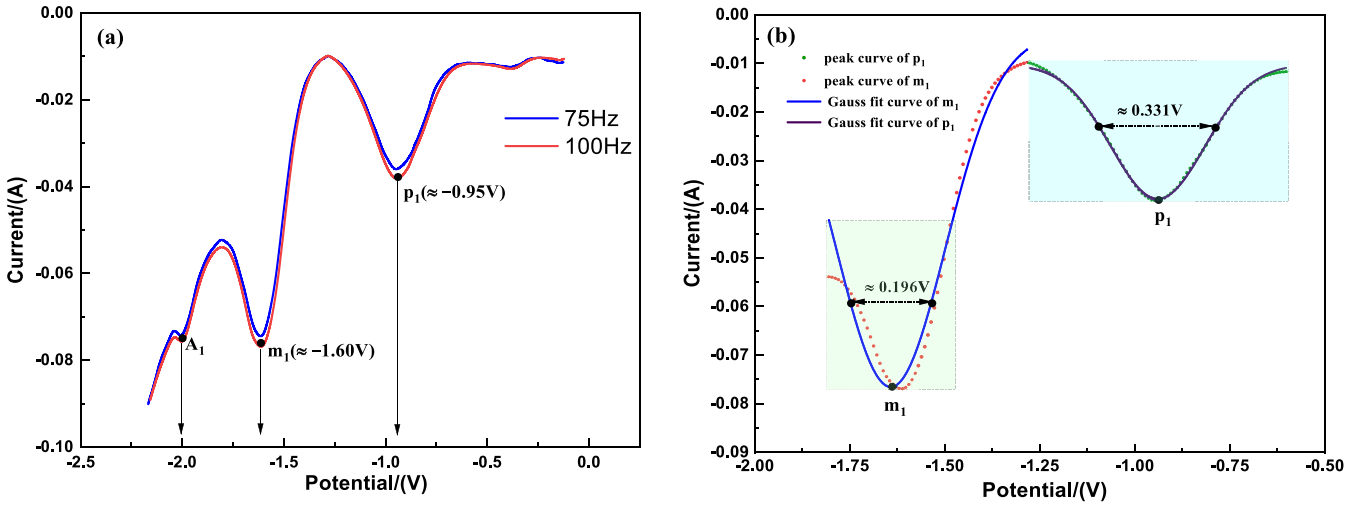

Figure 3. (a) Square-wave voltammetry curve and (b) Gaussian fitting of reduction peaks of $(LiF\text{-}LaF_3)_{eut.}$-$La_2O_3$(2 wt %) system (Temperature 1223 K; Pt reference electrode, Φ1 mm; Ni working electrode, Φ2 mm; W auxiliary electrode, Φ10 mm).

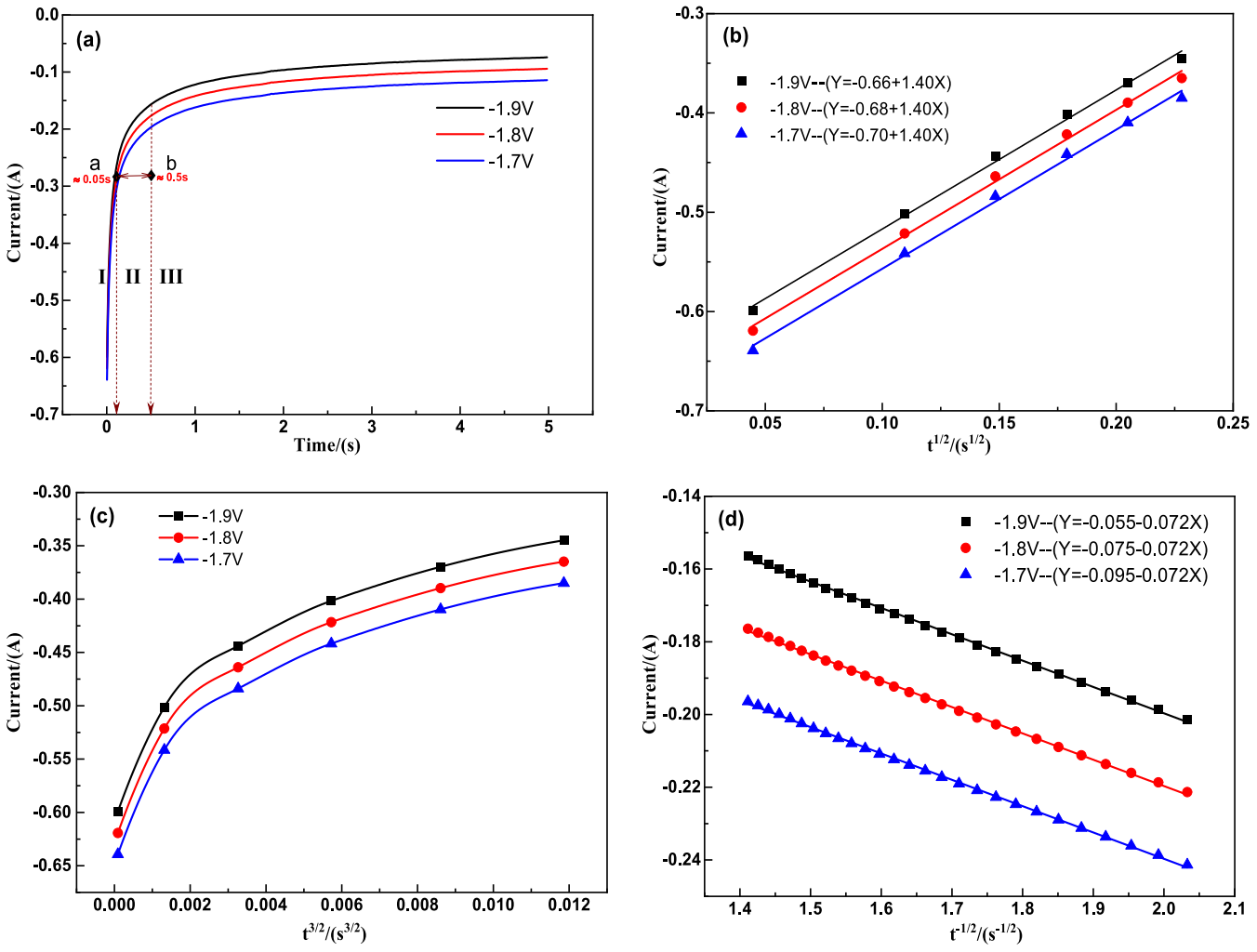

Figure 4. Square-wave voltammetry curve of (a) $(LiF\text{-}LaF_3)_{eut.}$-$La_2O_3$ (2 wt %) system and the relationship of (b) I–$t^{1/2}$ and (c) I–$t^{3/2}$ in phase I, (d)I-$t^{-1/2}$ in phase II.

square-wave voltammetry uses unidirectional scanning; therefore, the corresponding oxidation/reduction peaks cannot be displayed in pairs. Gaussian fitting of the peaks m_1 and p_1 at 100 Hz (Figure 3(b)) indicates their half-peak widths were 0.196 and 0.355 V, respectively. The number of electrons transferred during reduction that resulted in the peaks m_1 and p_1 are 1.89 (∼2) and 1.12 (∼1), respectively, as calculated by eq 1.[13]

https://doi.org/10.1021/acsomega.5c02626
ACS Omega 2025, 10, 25007−25013

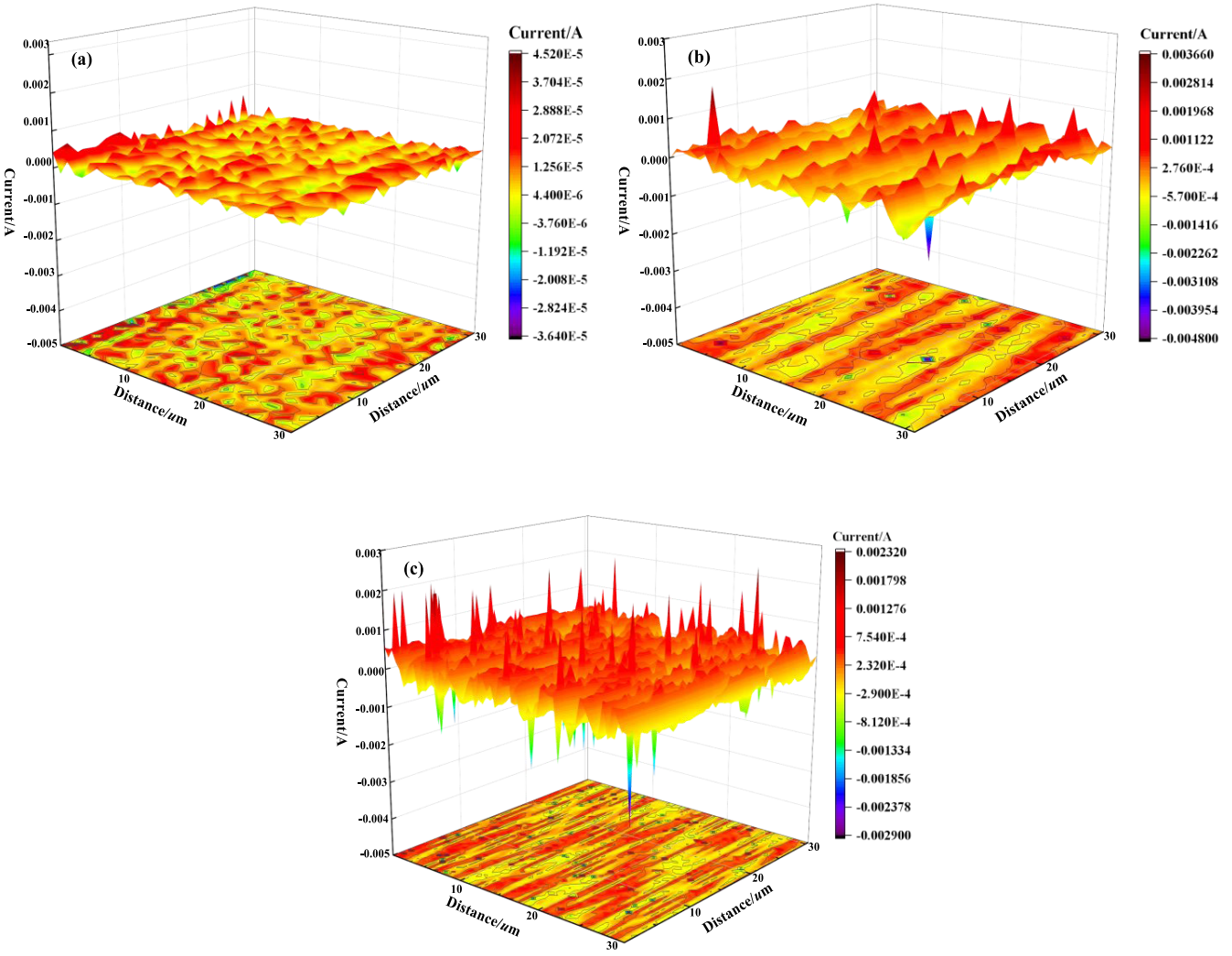

Figure 5. Response current projection diagram of Ni-based electrode in the potentials (a) [−0.25, 0.25 V], (b) [−0.60, 0.60 V], and (c) [−0.95, 0.95 V] ranges.

$$W_{1/2} = \frac{3.52RT}{nF} \quad (1)$$

Where $W_{1/2}$ is the half-peak width (V), R is the gas reaction constant (8.314 J·mol^{-1}·K^{-1}), T is the Kelvin temperature (K), n is the number of electron transfers, and F is the Faraday constant (96,485 C·mol^{-1}). Square-wave voltammetry analysis confirmed that the electrode reduction of La^{3+} ions proceeded in two steps, where p_1 represents the first step: $La^{3+} + e \rightarrow La^{2+}$, and m_1 represents the second: $La^{2+} + 2e \rightarrow La$.

3.1.2. Chronoamperometric Analysis. Diffusion and nucleation patterns of La^{3+} ions during electroreduction were analyzed using the chronocurrent method (Figure 4). The results of cyclic/square-wave voltammetry analyses show that the La^{2+} ions in the $(LiF\text{-}LaF_3)_{eut.}\text{-}La_2O_3$ system can be reduced to La, while Li^+ ions can be maintained in a stable state at potentials in the range of −1.6 → −2.0 V (vsPt). Therefore, excitation potentials of −1.70, −1.80, and −1.90 V (vsPt) were chosen for the chronocurrent analysis. The chronoamperometric curves of $(LiF\text{-}LaF_3)_{eut.}\text{-}La_2O_3$ system at different excitation voltages [−1.70, −1.80, and −1.90 V(vs Pt)] (Figure 4(a)) can be classified into the following three stages of reduction of La^{3+} ions at the Ni electrode.

3.1.2.1. Adsorption of La^{3+} Onto the Surface of the Ni Electrode. Phase I lasted for 0 to 0.05 s, and the current increased rapidly, which determined the La^{3+} ion adsorption and nucleation sites. According to the instantaneous and continuous nucleation eqs (eqs 2 and 3),[14] the $I\text{–}t^{1/2}$ and $I\text{–}t^{3/2}$ relationship curves shown in Figure 4(b,c), respectively, can be obtained from the data in Figure 4(a). I showed a linear variation with $t^{1/2}$ and a nonlinear one with $t^{3/2}$. Thus, it could be concluded that the nucleation mode of La^{3+} ions on the surface of the nickel electrode was transient.

3.1.2.2. Accelerated La^{3+} Reduction. Stage II lasted from approximately 0.05 to 0.5 s. The electrode process in this stage was controlled by diffusion of La^{3+} ions due to the fast rate of the reaction, $La^{3+} + e \rightarrow La^{2+}$, at the electrode. The chronocurrent curve of the $I\text{–}t^{-1/2}$ relationship (Figure 4(d)), indicates a fair linear relationship between I and $t^{-1/2}$, with a stable slope. The diffusion coefficient of La^{3+} ions in the system was calculated according to Cottrell's equation[15] and found to be approximately 1.33×10^{-5} cm^2·s^{-1}.

3.1.2.3. Diffusion-Reduction Equilibrium Phases of La^{3+} Ions. After 0.5 s, the diffusion rate of La^{3+} ions to the Ni cathode surface and the electron transfer process reached an equilibrium state and the current gradually stabilized.

https://doi.org/10.1021/acsomega.5c02626
ACS Omega 2025, 10, 25007−25013

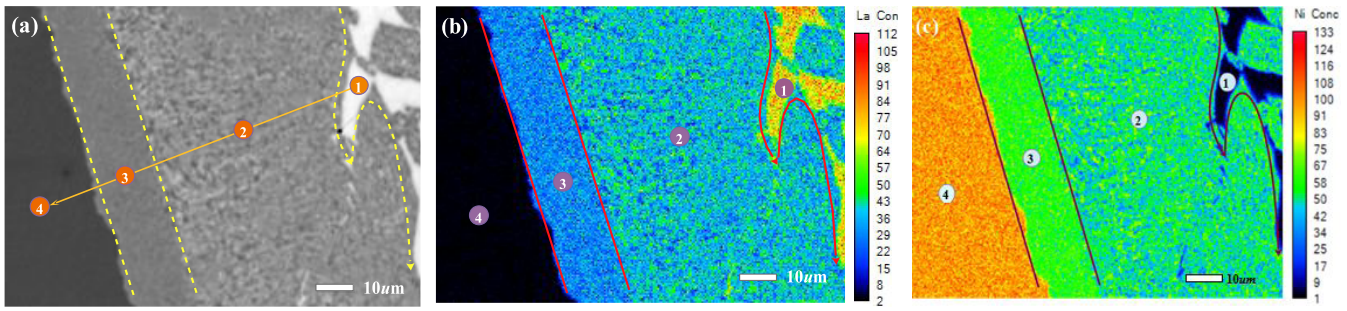

Figure 6. (a) SEM image of the microregion on the Ni cathode surface and the elemental distribution states of (b) La and (c) Ni.

$$I = \frac{ZFN_0\pi(2DC_0)^{3/2}M^{1/2}t^{1/2}}{\rho^{1/2}} \quad (2)$$

$$I = \frac{2ZFN_0\pi K_n(2DC_0)^{3/2}M^{1/2}t^{3/2}}{3\rho^{1/2}} \quad (3)$$

$$I = nFC_0SD^{1/2}\pi^{-1/2}t^{-1/2} \quad (4)$$

where I is the current intensity (A), n is the number of electrons transferred; C_0 is the concentration of La(III) ions (mol·cm^{-3}), F is Faraday's constant (96485 C·mol^{-1}), S is the immersion area of the working electrode (cm^2); D is the diffusion coefficient of La^{3+} ions (cm^2·s^{-1}),π is the circumference (3.14), t is the time (s), Z is the ionic valence state, K_n is the initial nucleation number, M is the relative atomic mass of the deposit (g·mol^{-1}); ρ is the density of the deposit (g·cm^{-3}).

3.2. Electrochemical Microanalysis of La^{3+} Ions on the Ni Cathode. The use of the SECM technique to analyze the current response of La^{3+} ions in an aqueous solution on the surface of a Ni electrode can provide more intuitive information for analyzing electroreduction of La−Ni alloys.[16] According to cyclic voltammetry analysis, the reduction potential of the La^{3+} + e → La^{2+} reaction is about −0.95 V. At a temperature of 298 K, the aqueous solvent is in a steady state in the 0 → −1.0 V potential range, while the reduction and oxidation potentials of Ni^{2+} ions are in the range −1.0 → 0 V and 0 → 1.0 V, respectively. Therefore, three potential intervals of [−0.25, 0.25] V, [−0.60, 0.60] V, and [−0.95, 0.95] V can be selected for SECM analysis of La^{3+} and Ni^{2+} ions in aqueous solution on the surface of the Ni electrode. The main purpose of the SECM analysis in an aqueous solvent at 298 K was to visualize the activation characteristics of La^{3+} ions and the Ni cathode, providing further insight into the electrode reaction mechanism in a high-temperature molten salt system.

Three ranges of potentials [−0.25, 0.25] V, [−0.60, 0.60] V, and [−0.95, 0.95] V (vs Ag/AgCl, hereafter) were applied to the microzone on the Ni-based cathode surface for a 0.01 mol/L $La(NO_3)_3$ solution at 298 K in the generate-and-collect mode. The variation in the surface-responsive current at the Ni electrode is shown in Figure 5. Figure 5(a) shows that the electrode response current lies in the interval [−0.001, +0.001] A within the scanning microregion when a potential in the range [−0.25, 0.25] V is applied to the Ni cathode substrate. Current projection maps show a diffused distribution of current without strong activation sites, indicating the presence of only a localized bilayer charge at the electrode, and discharge current formed by ions via adsorption−desorption. Figure 5(b) shows that the current within the scanned microregion increases to an interval of [−0.002, 0.002] A as the excitation potential of the Ni cathode extends to a range of [−0.60, 0.60] V. In the Ni^{2+} ion electrode reduction (i.e., Ni^{2+} + 2e → Ni), obvious active sites and current peaks appeared on the electrode surface and activated current regions appeared on the current projection map. When the applied potential was further extended to a range of [−0.95, 0.95] V (Figure 5(c)), the number and density of active sites on the Ni electrode surface increased considerably, the distribution range of the current-responsive points extended uniformly, and the intensity of the current peak also increased significantly to an interval of [−0.003, +0.003] A, along with the appearance of a clear strip-like active region in the current projection map. Two-dimensional and three-dimensional nucleation active sites coexisted in equilibrium on the Ni electrode surface, and La^{3+} ions were activated in this system. The negative current peak corresponds to the La^{3+} + e → La^{2+} electroreduction reaction, whereas the positive one corresponds to the La^{2+} ion desorption process. With a negative shift in the Ni cathode polarization potential, the strip-like two-dimensional nucleation region on the electrode surface expanded, and the three-dimensional nucleation sites increased and became distributed.

3.3. Reduction and Alloying Analysis of La^{3+} Ions on the Ni Cathode. To investigate the electrolytic reduction and alloying of La^{3+} ions on the Ni electrode surface, the products obtained upon electrolysis of the $(LiF\text{-}LaF_3)_{eut.}$-$La_2O_3$ system at 1223 K for 2 h at a constant cell potentiometric difference of 4.1 V were subjected to EPMA analysis (Figure 6). Nickel rods (Φ10 mm, 99.99%) and graphite rods (Φ10 mm, spectroscopically pure) were inserted into the electrolytic cell as the cathode and anode, respectively. Considering the La^{3+} ion reduction potential difference (above 1.60 V) and keeping the molten salt system stable (below 2.0 V), the potential difference that triggers the electrode reaction to proceed is controlled at 1.80 V. Meanwhile, the total resistance of the electrolyte system, electrodes, and connecting wires is about 0.035 Ω, and the power supply's output power is about 150 W, contributing the additional potential difference of about 2.3 V. As a result, the total potential difference of the electrolysis tank is about 4.1 V. Figure 6(a) shows the SEM image of the microregion on the Ni cathode surface (left side close to the center of the nickel electrode), and the contrast of coating shows four regions: ①white, ②off-white, ③gray, and ④gray-black. The EPMA composition was analyzed for each of the four regions (Figure 6(a), Table 1). The elemental distribution states of La and Ni were also analyzed (Figure 6(b,c)). Table 1 shows that the mass percentage of Ni in the black region④ in Figure 6(a) is 99.95% and La is absent, indicating that this region is the Ni electrode substrate part. The La/Ni atomic ratio in the adjacent region③ is 16.65/83.32 ≈ 1/5, and in region②, it is 25.13/74.68 ≈ 1/3. Similarly, the white region①, which is irregularly interspersed

https://doi.org/10.1021/acsomega.5c02626
ACS Omega 2025, 10, 25007−25013

Table 1. EPMA Compositional Analysis of the La−Ni Alloy

	mass percent (%)		mole percent (%)	
zone	La	Ni	La	Ni
1	92.27	7.56	83.25	16.32
2	45.68	54.15	25.13	74.68
3	32.17	67.56	16.65	83.22
4	0.00	99.95	0.00	99.92

with region②, appears as a La−Ni mixed region dominated by La, with a mass percentage of 92.27% La and 7.56% Ni. Based on the phase diagram of the La−Ni alloy system,[17,18] it can be inferred that alloying of zerovalent La, formed from electrochemical reduction of La^{3+} ions with an active Ni-based cathode, proceeds in two steps (eqs 5 reaction corresponds to formation of region② and (6) reaction corresponds to formation of region③), leading to the formation of Ni-rich main phases $LaNi_3$ and $LaNi_5$, respectively. It should be noted that part of the initially reduced zerovalent lanthanum in region① in Figure 6(a) can enrich on the Ni electrode surface to form a mix of La and La-rich phase (e.g., La_3Ni). However, as La continues to diffuse into the interior of the Ni electrode during the alloying process, a stable La-rich phase with Ni (e.g., La_3Ni, La_7Ni_3, LaNi, La_2Ni_3, and La_7Ni_{16}) cannot be formed due to the increase in the activity of Ni. According to the results of the electron microprobe analysis, the main impurity elements in the four organizational regions in Figure 6(a) show an increase in the level of O and trace amounts of C. The main source of O was the incomplete reduction of La_2O_3 during the electroreduction process, while the trace amount of C was mainly derived from the graphite electrolyzer and the carbon electrode. Therefore, it is not excluded that a small amount of La−Ni binary oxides and carbides will be interspersed in the alloy product. Lanthanide-rich intermediate phases (e.g., La_3Ni and La_7Ni_3) tend to liquefy at an electrolysis temperature of 1223 K. Thus, the best time to remove Ni from the La−Ni intermetallic compounds is to quickly strip the lanthanide-rich metal compounds that have formed on the cathode surface during the early stages of electrolysis. This process can be made more efficient by reducing the reaction surface of the cathode and increasing the current density.

$$La + 3Ni \rightarrow LaNi_3 \quad (5)$$

$$La + 5Ni \rightarrow LaNi_5 \quad (6)$$

Based on the above experimental results, it can be considered that it is feasible to separate rare earth lanthanum and samarium in lanthanum−samarium slag by electrolytic reduction in $(LiF\text{-}LaF_3)_{eut.}$-$La_2O_3$ system for the following reasons.

(1) The valence electron configuration of Sm is $4f^6 6s^2$, making it a typical variable-valence rare earth element. The Sm^{2+} ions formed by the reduction of Sm^{3+} ions during the electrolysis process are relatively stable and not easily further reduced at the Ni electrode.

(2) Rare earth samarium has a high vapor pressure, and it easily forms metal mist and volatilizes during the electrolysis process.

(3) The main components of lanthanum−samarium slag are La_2O_3 and Sm_2O_3, of which the mass percentage content of Sm_2O_3 is about 3%, and the activity in the electrolysis process is low. Generally, the solubility of corresponding rare earth oxides can only be enhanced by adding rare earth fluoride to the fluoride medium. However, $(LiF\text{-}LaF_3)_{eut.}$ medium does not contain SmF_3, resulting in the low solubility of Sm_2O_3 in the system and preventing it from competing with La_2O_3 for reduction.[61]

4. CONCLUSIONS

The electrochemical reduction of La^{3+} ions at the Ni cathode in the $(LiF\text{-}LaF_3)_{eut.}$-$La_2O_3$ system proceeds in two steps, i.e., $La^{3+} + e \rightarrow La^{2+}$and $La^{3+}+2e \rightarrow La$, and the electrode reaction is controlled by the diffusion of La^{3+} ions that is transiently nucleated on the Ni electrode surface. With a negative shift in Ni electrode potential, the $La^{3+} + e \rightarrow La^{2+}$ reaction area on the Ni cathode surface expands and the active sites increase and are uniformly distributed. La^{3+} ions present in the system can be fully activated when the potential is lower than −0.95 V. The La formed upon electrochemical reduction was alloyed with the active Ni-based cathode in a two-step alloying process, i.e., La + 3Ni → $LaNi_3$ and La + 5Ni → $LaNi_5$, to form Ni-rich $LaNi_3$ and $LaNi_5$ phases, respectively. Zerovalent La could not form a stable La-rich phase with highly active Ni on the electrode surface.

AUTHOR INFORMATION

Corresponding Author

Xu Wang − *College of Metallurgical Engineering, Jiangxi University of Science and Technology, Ganzhou 341000, China;* orcid.org/0000-0001-7051-6983; Email: 9120110061@juxst.edu.cn

Authors

Kailei Sun − *College of Metallurgical Engineering, Jiangxi University of Science and Technology, Ganzhou 341000, China*

Linsheng Luo − *College of Metallurgical Engineering, Jiangxi University of Science and Technology, Ganzhou 341000, China*

Complete contact information is available at: https://pubs.acs.org/10.1021/acsomega.5c02626

Notes

The authors declare no competing financial interest.

ACKNOWLEDGMENTS

This work was supported by the National Natural Science Foundation of China (No.52474328).

REFERENCES

(1) Huang, M.; Liu, K. J.; Zhang, H.; Zhang, X.; Li, J.; Xie, Y.; Lai, Y.; Huang, Z.; Qi, T. A novel process for the recovery of rare earth and fluoride compounds from calciothermic reduction slag. *JOM* **2023**, *75*, 3577−3586.

(2) Yi, W.; She, X.; Zhang, H.; An, Z.; Wang, J.; Xue, Q. Element migration and phase distribution characteristics during crystallization of rare earth phase in rare earth slag. *J. Rare Earths* **2023**, *41*, 780−788.

(3) Huang, J.; Zhang, L.; Yu, W.; Chen, J.; Le, C.; Ren, S. Extraction of rare earth and CaF_2 from rare earth calcium thermal reduction slag by using CaO roasting-acid leaching method. *Minerals* **2024**, *14*, No. 1001.

(4) Yin, T. Q.; Xue, Y.; Yan, Y. D.; Ma, Z.; Ma, F.; Zhang, M.; Wang, G.; Qiu, M. Recovery and separation of rare earth elements by molten salt electrolysis. *Int. J. Miner., Metall. Mater.* **2021**, *28*, 899−914.

(5) Chesser, R.; Guo, S.; Zhang, J. Electrochemical behavior of dysprosium and lanthanum in molten LiF-NaF-KF (Flinak) salt. *Ann. Nucl. Energy* **2018**, *120*, 246−252.

(6) Wang, Y.; Ge, J.; Zhuo, W.; Guo, S.; Zhang, J. Electrochemical extraction of lanthanum in molten fluoride salts assisted by KF or NaF. *Electrochem. Commun.* **2019**, *104*, No. 106468.

(7) Massot, L.; Gibilaro, M.; Nicaise, J.; Chamelot, P. Electrochemical behaviour of lanthanum fluoride and praseodymium fluoride on inert and reactive electrodes in molten LiF-CaF_2. *J. Fluorine Chem.* **2021**, *246*, No. 109797.
(8) Kim, G. Y.; Jang, J.; Paek, S.; Lee, S. J. Electrochemical removal of rare earth element in LiCl-KCl molten salt. *Sci. Technol. Nucl. Install.* **2020**, *2020*, 1−5.
(9) Xu, H.; Zhang, W.; Wang, C.; Yang, M.; Yan, T.; Yan, Y.; Zhang, M. Molten salt/liquid metal extraction: Electrochemical behaviors and thermodynamics properties of La, Pr, U and separation factors of La/U and Pr/U couples in liquid gallium cathode. *Appl. Radiat. Isot.* **2022**, *182*, No. 110149.
(10) Liu, Y.; Liu, Y.; Wang, L.; Jiang, S.; Wang, D.; Liu, Z.; Li, M.; Shi, W. Electrochemical behaviors and extraction of Ln(III) (ln = La,Ce,Nd) ions in LiCl-KCl-CsCl eutectic salts at low temperatures. *ACS Sustainable Chem. Eng.* **2023**, *11*, 8161−8172.
(11) Pan, J.; Yan, Y.; Deng, Y.; Wang, X.; Ding, L.; Kong, X.; Xue, Y.; Ma, F.; Zhu, K.; Liu, W. Electrochemical behavior and preparation of La-Ni Alloy in LaF_3-LiF-CaF_2-La_2O_3 molten salt on nickel electrode. *J. Phys. Chem. C* **2024**, *128*, 5816−5824.
(12) Zhang, Y.; Cai, B. Q.; Wang, X.; Wang, R.; Shi, Z. Electrochemical microscopy study of Yb (III) on the surface of a Ni cathode. *Ionics* **2023**, *29*, 345−352.
(13) Tang, H.; Pesic, B. Electrochemical behavior of $LaCl_3$ and morphology of La deposit on molybdenum substrate in molten LiCl-KCl eutectic salt. *Electrochim. Acta* **2014**, *119*, 120−130.
(14) Zhang, H.; Jiang, K.; Li, W.; Liu, Q.; Yu, J.; Zhu, J.; Yan, Y.; Zhang, M.; Wang, J. Electrochemical extraction of fission element samarium from molten NaCl-2CsCl eutectic salt using the liquid gallium cathode. *ACS Sustainable Chem. Eng.* **2023**, *11*, 8685−8698.
(15) Men, X.; Li, S.; Lv, Z.; He, J.; Song, J. Kinetic analysis of the cathodic reduction processes in molten salt electrolysis. *J. Alloys Compd.* **2024**, *1004*, No. 175785.
(16) Joo, M. H.; Park, S. J.; Hong, S. M.; Rhee, C. K.; Sohn, Y. Electrochemical recovery and behaviors of rare earth (La, Ce, Pr, Nd, Sm, Eu, Gd, Tb, Dy, Ho, Er, Tm, and Yb) ions on Ni Sheets. *Materials* **2020**, *13*, No. 5314.
(17) Okamoto, H. La-Ni (lanthanum-nickel). *J. Phase Equilib.* **2002**, *23*, 287−288.
(18) Dischinger, J.; Schaller, H. J. On the constitution and thermodynamics of Ni−La alloys. *J. Alloys Compd.* **2000**, *312*, 201−210.

https://doi.org/10.1021/acsomega.5c02626
ACS Omega 2025, 10, 25007−25013